MOVING CURRENT FILAMENTS IN ESD PROTECTION DEVICES AND THEIR RELATION TO ELECTRICAL CHARACTERISTICS

D. Pogany, S. Bychikhin, E. Gornik, M. Denison[#], N. Jensen[#], G. Groos[#+] and M. Stecher[#]

Institute for Solid State Electronics TU Vienna, Floragasse 7, A-1040 Vienna, Austria
[#]Infineon Technologies, Balanstrasse 73, D-81541 Munich, Germany
[+]University of Armed Forces, 85579 Neubiberg, Germany
+43-1-58801 36224; fax: +43-1-58801 36299; e-mail: dionyz.pogany@tuwien.ac.at

ABSTRACT

Dynamics and "travelling" modes of localized moving current filaments in electrostatic discharge (ESD) protection devices during current stress pulses are investigated using backside interferometric thermal mapping methods. The spatio-temporal evolution of the filament along the device width is related to the time evolution of the voltage waveform and to the IV characteristics of the device.

Keywords: ESD phenomena, current filament, thermal mapping, electrothermal effects, transmission line pulser, semiconductor device testing

INTRODUCTION

Inhomogeneous current flow or current filamentation is a main failure cause in power devices [1,2] and electrostatic discharge protection devices (ESD PDs) [3-5]. Destructive filaments are formed during second breakdown event due to positive thermal feedback and thermal carrier generation [6,7]. Filaments may also have a pure electrical origin, driven by instabilities related to a negative differential resistance (NDR) in S-shaped current voltage characteristics [8-11].

Current spreading mechanisms and pulse to pulse instabilities in current distribution in ESD PDs have previously been studied using a scanning [12] as well as a 2D interferometric technique [13,14]. Under high stress magnitudes, large filaments (or current inhomogeneities) were observed. Under sufficiently long stress duration, the active region was observed to spread over the whole width of the investigated devices. A monotonic increase of the device voltage accompanies the current homogenization process during the stress pulse. This indicates that the homogenization process is related to the negative temperature dependence of the impact ionization coefficient. In effect, in order to maintain the constant current value during the stress pulse, the voltage has to increase to assure the same generation rate.

In this contribution the dynamics and "travelling" modes of localized current filaments in smart power ESD PDs are investigated. We combine backside transient interferometric mapping (TIM) techniques (scanning [15,16] and holographic [13,14]) with detailed electrical measurements. In contrary to the previous studies we concentrate to lower stress currents and longer pulse lengths. Under such conditions, the filament remains well localized and moves during the pulse, i.e. no current homogenization occurs. The filament "travelling" in the device produces a specific "fingerprint" in the measured voltage waveform. Consequently a specific pattern is formed in the IV characteristics, when plotted point by point. Such an electrical behavior is usually hidden in standard ESD testing due to data averaging over time and over different stress pulses. Filament "travelling" modes and mechanisms are investigated in two different device types, which exhibit a single and complex filamentary behavior.

DEVICES STUDIED

Smart power technology ESD protection test structures are fabricated on an n-epi layer grown on a p-substrate (see Fig. 1). A p-well / n-buried layer pn junction determines the breakdown voltage in both devices (about 40V, V_{HBM}>8kV). A n^+ - sinker is used as a collector contact. A n+ diffusion in the p-well forms the emitter of the vertical npn transistor of the npn ESD protection device (see Fig. 1a and [12,17]). The p-base and n-emitter are short-circuited.

A Silicon Controlled Rectifier (SCR) device is formed by adding an p-doped region close to the sinker of a npn device. In this way a lateral pnp transistor is created which is connected to a vertical npn one as indicated in Fig. 1b [18,19].

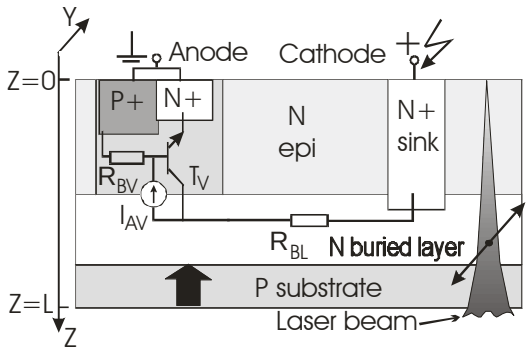

(a)

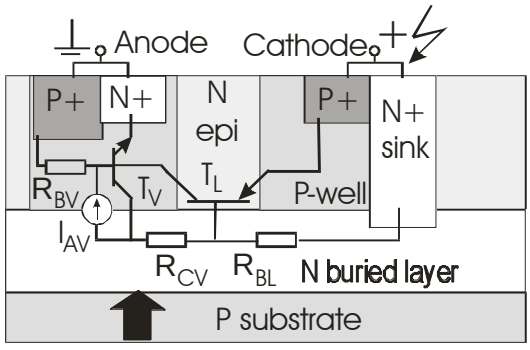

(b)

FIGURE 1. *Simplified cross section with an electrical replacement scheme of a npn (a) and SCR (b) ESD protection device. The black arrows indicate the position of the phase maxima along the device length.*

METHODS

Optical methods

The current-induced power dissipation is studied by monitoring the temperature-induced changes in silicon refractive index by an infrared probe beam. The resulting optical phase shift Dj is detected interferometrically using the TIM method. A scanning interferometer [15] is used to obtain the time evolution of phase shift at each position with 3ns-resolution. A focused infrared probe laser beam is used (wavelength λ=1.3um, space resolution 1.5μm) to scan the device along the device width (*y*-direction, see Fig. 1a). The beam is positioned at the maximum phase shift along the *x*-direction. Typically 3-50 pulses are applied at each position in order to monitor all possible phase distributions (filament "modes"), which may vary from pulse to pulse. A similar approach, employing "scatter" plots of phase shift, has previously been used to study current spreading phenomena and pulse to pulse instabilities in ESD PDs [12].

A 2D TIM method is used to capture the temperature-related phase image of the whole device [13]. This method uses the principle of holographic interferometry where a broad laser probe beam (λ=1.3um) illuminates the whole active area from the device backside. The thermal distribution in the device can be obtained during a single stress pulse with a time resolution of 5ns. This method permits us to distinguish unambiguously between different filament modes.

If the thermal effects dominate, which is the present case (the free-carrier contribution to the total phase shift can be neglected or can be spatially separated from the thermal contribution), the phase change Dj is directly related to a 2D thermal energy density E_{2D} in the device [16]:

$$E_{2D}(x,y,t) = \frac{\lambda\, c_V}{4\pi\, dn/dT}\Delta\varphi(x,y,t) = 0.88\,\Delta\varphi \qquad (1)$$

where c_V is the volume specific heat, dn/dT is the thermo-optical coefficient, and E_{2D} and Dj in the numerical expression are in nJ/μm^2 and rads, respectively. E_{2D} is in fact a projection of 3D thermal energy density $c_V DT$ to the lateral plane $\{x,y\}$, where DT is the difference between the temperature due to self-heating and the room temperature. As such E_{2D} and therefore also the phase shift is a memory quantity reflecting all the previous time-dependent distributions of power dissipation in the device.

The instantaneous 2D power dissipation density P_{2D} (i.e. a 2D projection of a 3D power dissipation density) can be calculated from the time and second-space derivative of the measured phase shift [19,20]. Neglecting small voltage variations on the device, P_{2D} represents well the local current density in the device. More precisely, it is an averaged current density over the laser beam path. Using "scatter" data of phase shift, where two or more space distributions of the phase shift overlap, only a time derivative can directly be calculated. Therefore P_{2D} is calculated neglecting the space derivative terms [19]:

$$P_{2D}(x,y,t) = \frac{\lambda}{\frac{dn}{dT}}\frac{c_V}{4\pi}\frac{\partial\Delta\varphi(x,y,t)}{\partial t} \qquad (2)$$

Intuitively, taking into account (1), P_{2D} is nearly a time derivative of E_{2D}. P_{2D} calculated using (2) describes well the dynamics of the current filaments. The neglecting of the space derivative term in expression for P_{2D} introduces undulations in P_{2D} (can be negative, see below).

Electrical stress

The devices are stressed by current pulses with constant amplitude and 500 ns - 1μs duration. A transmission line pulser (TLP) [21] and a high power switch [15] were used. The stress drives the devices into a bipolar snapback mode where the avalanche multiplication in the base-collector junction supports the electron injection from the emitter-base junction of the vertical npn transistor. In the SCR device, at the low stress currents used, only the vertical npn transistor is active and the lateral pnp transistor is not triggered.

Using both scanning and 2D TIM methods, at each stress pulse a voltage waveform *U(t)* was recorded. It was correlated with the phase evolution $Dj(t)$ at a particular position $\{x,y\}$ in the case of scanning method. In the case of 2D holographic method *U(t)* was correlated with the phase distribution $Dj(x,y)$ at a particular time window around *t*. By this way it was possible to relate the *U(t)* evolution during the pulse with a particular spatio-temporal evolution of the current density in the device.

The IV characteristics were obtained by averaging the current and voltage waveforms in a short time interval (usually some 2-5ns). The undulations in the waveforms due to unmatched load vanish after some 50ns. Therefore, for longer times the measured voltage directly represents the voltage due to instantaneous internal device behavior.

RESULTS AND DISCUSSION

Localized moving current filaments are observed in devices exhibiting a NDR or a near-zero differential resistance region in the high current IV curve. The filament characteristics (starting place, size, speed, "travelling mode" and occurrence probability of the mode) depend strongly on stress magnitude. We emphasize that no relation has been found between the filament behavior and a particular device type (for example npn or SCR). A common feature observed is that the filament complexity (number of filament modes) was usually found to increase with increasing stress current. In the following we present typical characteristics of simple (one single dominant mode) and more complex current filaments, which were observed in the studied devices.

Simple filaments

Figure 2a shows the "scatter" plot of phase distribution (thermal energy) along the width of a SCR device for five particular time instants during a 1μs long stress pulse of magnitude I_S=0.15A. Figure 2b represents the extracted P_{2D} data (i.e. representing the current density), obtained using (2), for the same time instants. At the pulse beginning (t≤100ns) only one localized peak (current filament) can be seen in both Dj and P_{2D} distributions, which indicates that the current starts to flow in the device center. The filament stays at the same place, and the phase shift, and therefore temperature, increases with time. At further times (t>100ns), the Dj scatter plot forms two overlapping "envelop" distributions (see the plot at t=200ns in Fig. 2a). In the P_{2D} plot, two well-separated localized regions can be distinguished. From the P_{2D} data we can estimate the filament size to be less than 10μm.

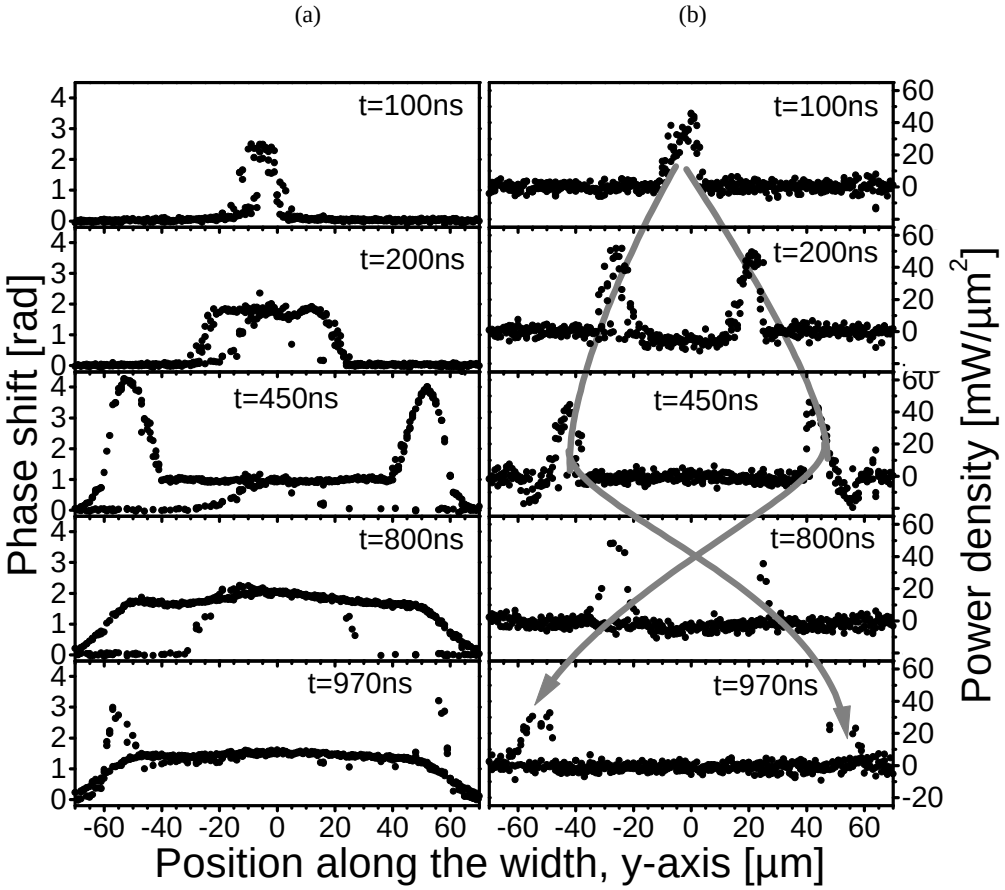

FIGURE 2. *Scattered plots of (a) Dj and (b) P_{2D} distributions along the width of a SCR with time as a parameter; I_S=0.15A. The scanning interferometer is used. At each position the data for several stress pulses are presented. The two envelopes obtained from the data points represents two equivalent symmetrical filament modes (only one filament exists during the stress pulse). The negative undulations in P_{2D} are artifacts arising from the neglecting of space derivative terms in calculations. The solid gray lines in (b) indicate how the filaments move with time.*

The above results show that (i) the original current filament starts to move from the center toward corners, and that (ii) the direction of the movement toward corners is random from pulse to pulse. It can also be noticed from Fig. 2a that the phase shift at t=100ns is higher than at t=200ns. It means that the temperature in the filament for t≤100ns, when the filament does not move, is higher than for t>100ns, when it moves.

The filament reaches the corner at time t≈350ns after the pulse beginning. It stays some time at the corner and starts to move back towards the opposite device corner. At the corner the phase shift increases, indicating that the temperature in the filament at the corner exceeds the temperature in the filament when it moves. The current filament reaches the opposite corner at t≈950ns after the pulse beginning. Similarly as during the first turn-around the corner, it stays some time at the corner and then starts to return back. The two gray lines in Fig. 2b represent two possible filament paths in the device with progressing time.

At this point we would like to point out the "memory" property of phase shift. While P_{2D} shows that the position of filament is well localized, the phase shift distribution is non-zero even in regions where P_{2D}=0. The amplitude of phase shift in the region with P_{2D}=0 depends well on the rate of cooling to lateral sides and on filament size [16]. The phase dynamics during cooling can well be seen in the time evolution graph in Fig. 3. Here $Dj(t)$ is shown in the middle (y=0μm, cf. Fig. 2) and near one corner (y=40μm) of the device. In these records, the filament moves first from position y=0 to the position y=60um and then returns back. The Dj increase means that the filament dissipates heat at the measurement position, while the Dj decrease means the cooling. At position y=0μm the phase increases immediately from the pulse beginning (t=0ns), as the filament originates there. When the filament leaves the device center, the cooling occurs. Then around t=630ns, the filament passes again the device middle (cf. also Fig. 2b, P_{2D} data at t=450ns and 800ns). At position y=40μm in Fig. 3, the heating starts with a delay and two closely-in-time spaced phase rises can be observed due to two-fold passage of the filament over this position.

It should be noted that the cooling rate ($|dDj/dt|$) in the filament is quite high (see decreasing part of Dj(t) in Fig. 3) as the filament is well localized in space and the heat can spread to both lateral directions (i.e. parallel and perpendicular to device width). In case when the device triggers homogeneously along the width (i.e. the longer dimension) and the probe beam position is far (compared to diffusion length) from sample corners, the phase decreases much more slowly (see e.g. [16]). This is caused by the fact that in the latter case the heat can spread only in one lateral spatial direction (i.e. along the device length - shorter device dimension along the x-axis).

Phase distributions due to the heat generation in filament, recorded by the 2D TIM method at two time instants, are shown in

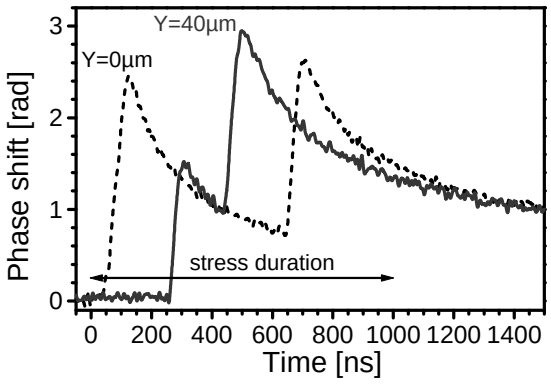

FIGURE 3. *Phase shift evolution at two different positions in the SCR device.*

Fig. 4. At t=200ns after the pulse beginning, the phase shift exhibits a localized plateau beginning at the device center (Fig. 4a), which is consistent with the results of Fig. 2a. The phase profile in Fig. 4b is recorded at the moment where the filament returns back from one device corner. One can clearly see a comet-like tail in the phase distribution between the center and corner of the device. As well, a phase shift peak is observed at the corner. The measured phase profiles are consistent with the scanning TIM measurements in Fig. 2a. It can also be noticed that the phase shift along the device length (x-direction) peaks at the position related to the n+ emitter, confirming that only the vertical npn transistor is active under the stress conditions used.

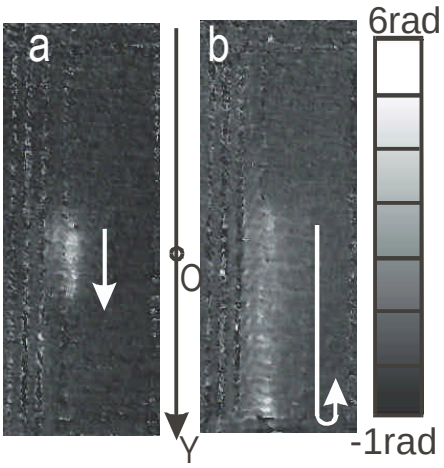

FIGURE 4. *Single-shot 2D phase images of SCR device at I_S=0.15A, recorded at time (a) t=200ns and (b) t=400ns after the pulse beginning. The arrows indicate the filament movement.*

The voltage waveform related to filament movement in Fig. 2 is shown in Fig. 5 (see *U(t)* at I_S=0.15A). As long as the filament stays at the position of its origin (center of the device), the voltage of the device increases (t<100ns). As the filament moves to corner, the voltage lowers and remains nearly constant until the filament approaches the corner (t<270ns). When the filament is some 10µm away from the corner, the voltage on the device abruptly decreases (the minimum is marked by (-) at t≈320ns in the curve for I_S=0.15A, see Fig. 5). At the corner, when the filament stays, the voltage across the device rapidly increases (maximum marked by (+) in Fig. 5). When the filament returns the voltage lowers and remains nearly constant during the time the filament moves to the opposite corner. As the filament approaches and reaches the opposite corner, the same features as described above are observed: First the voltage decreases and then the voltage increases (see marking by (-) and (+) in the time interval of 870 - 950ns in Fig. 5).

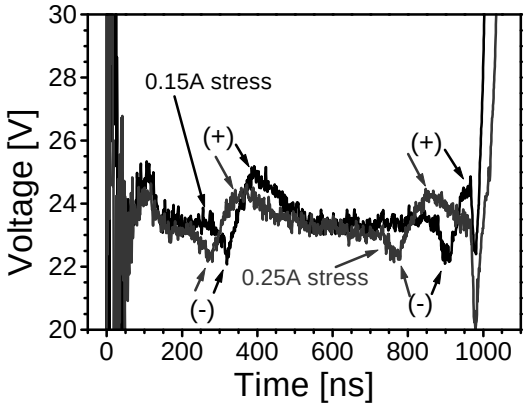

FIGURE 5. *Vertical zoom of the voltage waveforms in the SCR devices under 1µs long current pulses of 0.15A and 0.25A. The indicated voltage decrease (-) and increase (+) is related to the filament passage just before the corner and at the corner, respectively.*

It should be noted that the voltage waveform *U(t)* in Fig. 5 at I_S=0.15A is common for both movement directions of the filament. This is due to the symmetry of the device and of the filament modes.

The filament speed was found to increase with the stress current. Fig. 6 shows the extracted P_{2D} distribution at I_S=0.25A at time t=800ns. Compared with the P_{2D} distribution at the same time instant for I_S=0.15A (Fig. 2b), it can be seen that the filament at I_S=0.25A travels longer distance (i.e. it is closer to either corner). This effect can also be seen in Fig. 5 where the voltage waveform for I_S=0.25A is also shown. The voltage minima (-) or maxima (+) in *U(t)*, related to filament passage over the corner, occur earlier at I_S=0.25A compared to that at I_S=0.15A. It can be noted that more complex modes with low occurrence probability were observed in this device at higher stress current (not discussed here).

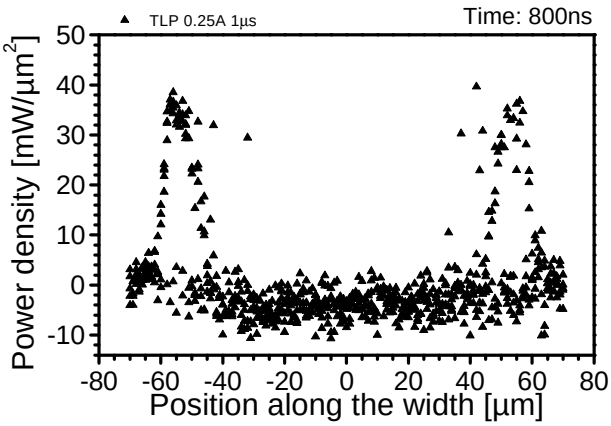

FIGURE 6. *Extracted P_{2D} distribution in the SCR device at I_S=0.25A and t=800ns. The filament travels a longer path compared to that at lower stress currents (compare with P_{2D} distribution at t=800ns@ 0.15A in Fig. 2b). The randomly occuring points outside of the dominant filament region are due to another rare filament mode.*

Fig. 7 shows the IV curve of the SCR device at low currents plotted at two time instants. The averaging is performed only at time interval of 2ns. The time variation in *U(t)* results in temporal variations in IV curve. A crossover between the IV curves recorded at different time intervals can be observed. This is a fingerprint of specific internal device behavior, exhibiting moving current filaments.

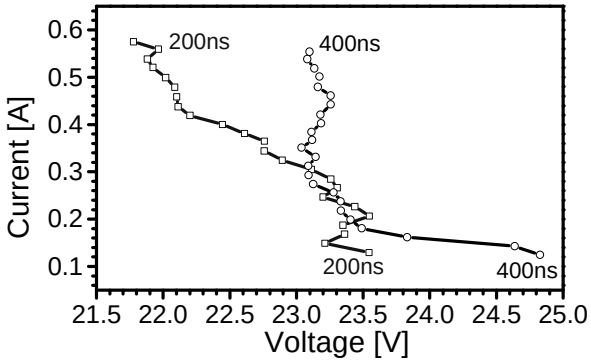

FIGURE 7. *High current IV curves for the SCR device at two different time instants.*

Interpretation: From the increase of filament speed with I_S (i.e. also with dissipated power) it can be concluded that the driving force for the filament movement is the temperature rise or more precisely the temperature gradient in the filament. In other words, the filament moves from hotter to cooler region. This is caused by the negative temperature dependence of impact ionization coefficient [12,22].

The voltage decrease related to the filament position just before the corners is attributed to a higher impact ionization rate at terminations (spherical junctions). The voltage increase at the corners, where the filament stays, is attributed to the increased temperature there. Consequently, in order to maintain the constant impact-ionization generated current, the voltage has to increase. As the filament moves, the voltage remains nearly constant, since the walking has a stabilizing effect on the filament temperature.

The strong filament localization, as opposed to the current homogenization at higher currents [12] is attributed to the combined effect of the NDR-related electrical non-linearities and low applied current on one hand, and thermal dynamics on the other hand:

1. Due to NDR, the current density in the device becomes unstable with respect to small fluctuations in carrier density, producing current collapse into a filament [8,11]. When the total applied current is low, the current filament has a small size.

2. Due to the small filament size, the cooling to lateral sides is fast (see the discussion related to Fig. 3). The low dissipated power and the filament movement cause that the temperature along the device width cannot homogenize, at least for times less than 1μs. Therefore the current flow cannot homogenize and it remains strongly localized. The current density in the filament is nearly constant with time (see nearly the same P_{2D} maxima in Fig. 2b). It should be noted that at high power dissipation (I_S>1A [18]), the temperature along the width homogenizes quickly as the thermal energy input in the device active area overcomes the energy output due to lateral heat spreading. This results in the fast current flow homogenization, i.e. initially spatially localized filament increases its size (decreases the current density) with time, up to the device width.

On the other hand, the pulse to pulse instabilities in the filament direction are supposed to originate from small fluctuations in the carrier density in the device center.

Complex filaments

Figs. 8 and 9 show a "scatter" plot of the phase shift and P_{2D} distributions along the width of the npn device at t=200ns and t=400ns, respectively (I_S=0.5A). In this device, two *dominant* symmetrical filament modes (so in total four modes) are found. In both modes the filament originates close to one of the device corners. The filament position randomly alternates between the two corners from pulse to pulse. The original width of filament is approximately 30μm. The characteristics of the two modes are presented in the following:

Mode 1. The maximum of the phase shift at the position of filament origin peaks some 15μm from the corner (see Mode 1 in Fig. 8). The occurrence probability of this mode is 50%. With progressing time the filament stays nearly at the original position, while the phase amplitude, and therefore also temperature, increases (see Fig. 9). The center of the filament (defined as peak in P_{2D} distribution) moves slightly toward the corner. The P_{2D} peak position as a function of time is schematically shown in Fig. 10.

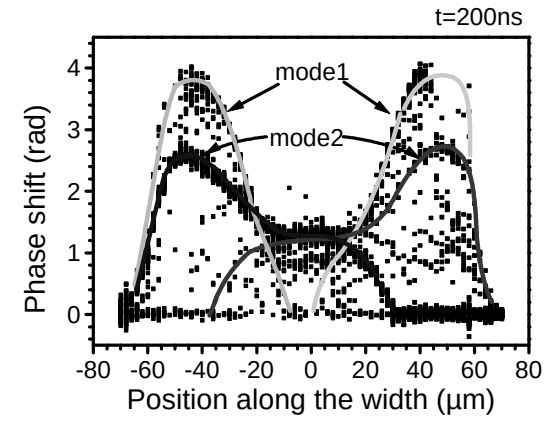

(a)

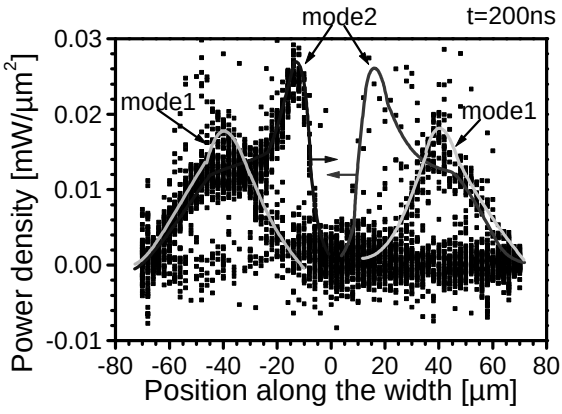

(b)

FIGURE 8. *Scattered plot of (a) phase shift and (b) P_{2D} in the npn device at t=200ns and I_S=0.5A. Two dominant non-equivalent symmetrical modes (i.e. in total four) are indicated by solid lines "envelopes".*

The phase distribution at two time instants, obtained using the 2D TIM method is shown in Fig. 11. It can clearly be seen that the spatial extent of the filament at *t*=125ns (Fig. 11a) remains almost unchanged compared to that at *t*=400ns (Fig. 11b). However the phase amplitude at *t*=400ns increases, which is consistent with the scanning TIM measurements (see Fig. 8a and 9a).

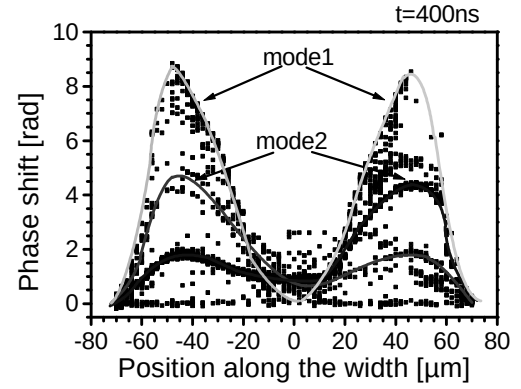

(a)

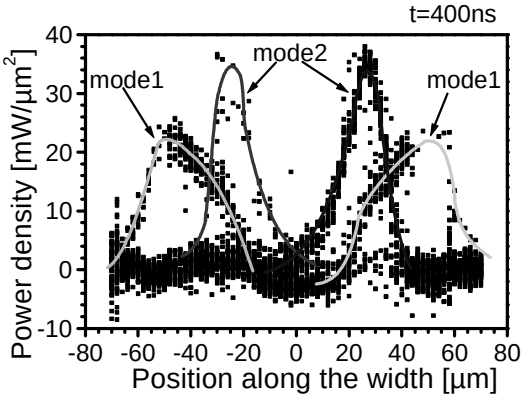

(b)

FIGURE 9. *Scatter plot of (a) phase shift and (b) P_{2D} in the npn device at t=400ns; I_S=0.5A.*

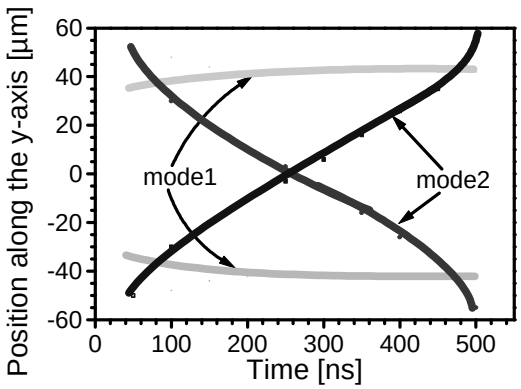

FIGURE 10. *Sketch showing the evolution of the possible filament modes in the npn device. Only the position of the filament center is plotted.*

The voltage waveform related to this mode is shown in Fig. 12 (curve Mode 1). One can see a monotonous increase of the device voltage from the pulse beginning. This is attributed to the strong heating and temperature increase in the filament, which does not move, and a consequent decrease of impact ionization rate.

Under pulses of 500ns duration following Mode 1, one can sometimes observe a sharp decrease in the voltage some 10-20ns before the pulse end (see the arrow in Fig. 12). This is attributed to a second breakdown event [6,23], which is however non-destructive (see e.g. [14] for non-destructive 2nd breakdown events). It means that no increase in leakage current was observed after such an event. In this case, the voltage drop would be related to the onset of thermal generation of holes at the position of temperature maximum in the filament [7].

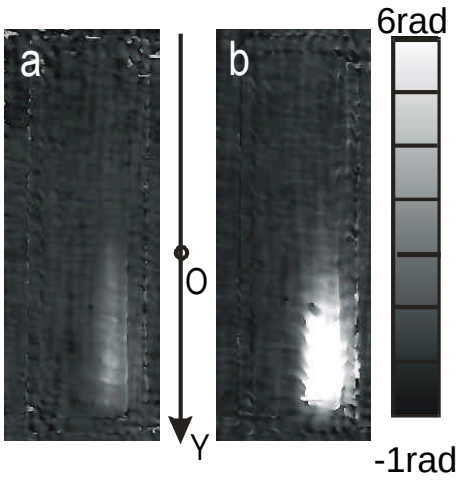

FIGURE 11. *Single-shot 2D phase images in the npn device, related to filament Mode 1 at two time instants: (a) t=125ns and (b) t=400ns.*

Mode 2. In the second filament mode (occurrence probability is 45%), the current filament originates at the either corner, as well. With progressing time the filament moves toward the opposite device corner where it stays for some time (see Figs. 8 and 9). The evolution of P_{2D} peak for this mode is schematically shown in Fig. 10 (see curve "Mode 2"). At the end of the 500ns long pulse, the filament reaches the opposite corner. For prolonged pulses or slightly higher stress magnitude the filament can return back, similarly as in the results of Fig. 2. As well, the filament speed increases with the input power magnitude. This is consistent with the previous results, where the spreading speed of a large current filament (i.e. speed of homogenization of current flow along the device width) under high current stress (I_S>1A) was found to increase with dissipated power [12,13].

The voltage waveform related to "Mode 2" is shown in Fig. 12. During the time the filament moves toward the opposite side the voltage is nearly constant. As the filament reaches and stays at the corner, the voltage starts to increase. This is due to a temperature increase in the filament. The above results are consistent with the behavior of *U(t)* related to the simple filament (Figs. 2 and 5), therefore the same explanation can be applied.

Very rarely (occurrence probability 5%), the Mode 1 can change to Mode 2. The filament stays in one device half until some 300 ns - 350 ns and then it starts to move toward the opposite corner. The voltage waveform related to this mode is shown in Fig. 12 (see curve "Mode 12"). During the time the filament stays at one device half the voltage increases. When the filament passes to another device half (i.e. transition to cooler region), the voltage abruptly decreases and remains nearly constant while the filament moves. This is similar to the previously mentioned results. This also suggests that a potential barrier in the device center exists for the passage of current from one

device half to another. The existence of such a barrier would explain why the current can stay in one device half for longtime in Mode 1.

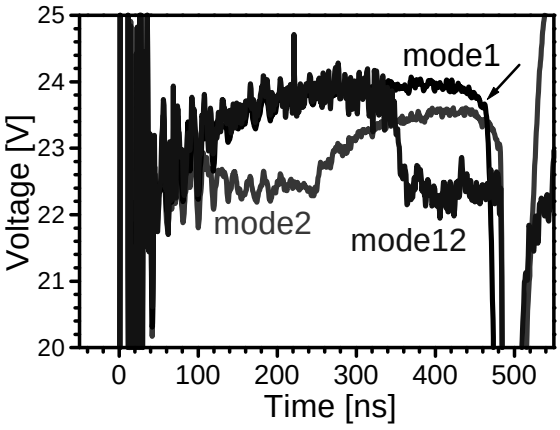

FIGURE 12. *Three typical U(t) waveforms which corresponds to particular filament modes (Modes 1 and 2 are dominant, and Mode 12 is rare).*

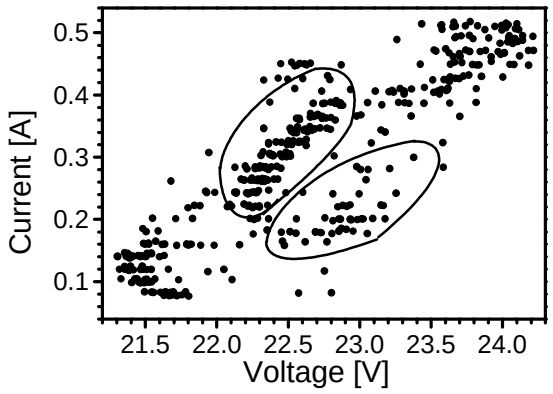

(a)

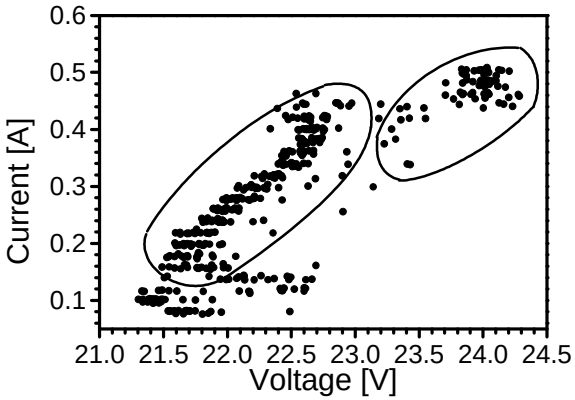

(b)

FIGURE 13. *Scatter plot of IV curve at time (a) t=350ns and (b) t=450ns after the beginning of stress pulse in the npn device. Twenty measurements are performed for each stress level. The voltage values "cluster" in branches (marked by ovals) which corresponds to different filament "travelling" modes.*

We hypothesize that fluctuations in current density/carrier concentration in the first moment of device triggering (i.e. at the pulse risetime) determines which filament mode realizes. If the device triggers at the corner, Mode 2 realizes. If the device triggers closer to the middle, but still near the corner, mode 1 or 12 realizes. The initial current distribution results in a particular initial temperature profile in the device, which then may control the current flow modes at later times.

Fig. 13 shows a scatter plot of the IV curves plotted at *t*=350ns and *t*=450ns after the pulse begin. The variations in the filament mode (so variations in *U(t)*) from pulse to pulse result in the scattering of the IV data points and their clustering according to their statistical weights. The clustered data form branches (marked by ovals) in the IV curves, which are related to specific filament modes. So the scattering and clustering in the IV indicates that the device exhibits physically different internal behavior from pulse to pulse.

CONCLUSIONS

Strongly localized moving current filaments have been found in ESD PDs at low stress levels. Each filament "travelling mode" produces a unique fingerprint on the *U(t)* curve. The decrease in voltage occurs when the filament approaches a region with higher impact ionization rate (e.g. terminations) or when it passes from a hot region into a cooler region. The voltage increase is attributed to an increase of temperature at the filament position. It occurs typically when the filament does not move, e.g. at the corner. A constant voltage during the current pulse is typically observed when the filament moves. This is due to a stabilizing effect of filament movement on its temperature.

The voltage variations due to filament dynamics cause particular temporal variations in device IV curves. Moreover, when pulse to pulse variations in filament "travelling mode" exist, several branches may appear in IV curves. This IV pattern can evolve with time, due to filament movement.

We propose to measure IV curves by averaging the voltage waveform only in a limited time interval. Several pulses should be applied for the same stress level and the data have to be plotted point by point. This allows the identification of possible pattern in the IV curves, which could indicate a complex device behavior. Even if in the present devices the current filamentation at low amplitude stress has no influence on their ESD robustness (>8kV Human Body Model), the proposed IV analysis may be important at the early stage of device development. The electrical characterization alone may already reveal the existence of different "triggering" or filament modes, which may be related to a particular failure mode. The above IV analysis may also be applied to multifinger devices, where the voltage variations or clustering would indicate a complex and unstable current flow over or between single fingers.

Acknowledgements

The work has been supported by European Community project DEMAND IST2000-30033. Pavel Rodin from Ioffe Physicotechnical Institute, Russian Academy of Sciences in St. Petersburg as well as from Institute for Theoretical Physics, TU Berlin is gratefully acknowledged for fruitful discussions on physics of moving filaments and nonlinear dynamics in general.

REFERENCES

[1] M. Stoisiek, G. Wachutka and D. Theis "2D simulations and experiments on avalanche injection in GTOs", in *Proc. Int. Symp. Power Semicond. Dev. and ICs 1998*, Tokyo, 1988, pp. 48-55.

[2] M. Domeij, B. Breitholtz, M. Östling, J. Lutz: "Stable dynamic avalanche in Si power diodes", *Appl. Phys. Lett.* vol. 74, 1999, pp. 3170-3172.

[3] C. Duvvury, C. Diaz, and T. Haddock, " Achieving uniform nMOS device power distribution for sub-micron ESD reliability", in *IEDM'92 Techn. Dig.*, pp. 131-134.

[4] C. Russ, K. Bock, M. Rasras, I. De Wolf, G. Groeseneken, and H. E. Maes, "Non-uniform triggering of gg-nMOSt investigated by combined emission microscopy and transmission line pulsing", in *Proc. EOS/ESD Symp. 1998*, Reno (USA), pp. 177-186.

[5] P. Salome, C. Leroux, J. P. Chante, P. Crevel and G. Reimbold, "Study of a 3D phenomenon during ESD stresses in deep submicron CMOS technologies using photon emission tool", In *Proc. IRPS'97*, pp. 325-332.

[6] W. B. Smith, D. H. Pontius, and P. P. Budenstein, "Second breakdown and damage in junction devices", *IEEE Trans. Electron Dev.*, vol. 20, 1973, pp. 731-744.

[7] A. Amerasekera, J. A. Seitchik, "Electrothermal behavior of deep submicron nMOS transistors under high current snapback (ESD/EOS) conditions" In *IEDM'94 Techn. Digest*, 1994, pp. 455-458.

[8] E. Schöll, *Nonequilibrium phase transition in semiconductors*, Springer 1987.

[9] V. A. Vashchenko, Y. B. Martynov, and V. F. Sinkevitch, "Electrical instability and filamentation in ggMOS protection structures", *Solid-St. Electron.*, vol. 41, 1997, pp. 1761-1767.

[10] F.-J. Niedenostheide, B. S. Kerner, H. -G. Purwins, "Spontaneous appearance of rocking localized filaments in a nonequilibrium distributed system", *Phys. Rev. B.*, vol. 46, 1992, pp. 7559 - 7570.

[11] A. Alekseev, S. Bose, P. Rodin, E. Schöll, "Stability of current filaments in bistable semiconductor systems with global coupling", *Phys. Rev. E*, vol. 57, 1998, pp. 2640-2649.

[12] D. Pogany *et al.*, "Study of trigger instabilities in smart power technology ESD protection devices using a laser interferometric thermal mapping technique", in *Proc. EOS/ESD Symp. 2001*, pp. 216-227.

[13] D. Pogany, V. Dubec, S. Bychikhin, C. Fürböck, M. Litzenberger, G. Groos, M. Stecher, E. Gornik, "Single-shot thermal energy mapping of semiconductor devices with the nanosecond resolution using holographic interferometry", *IEEE Electron Dev. Lett.*, vol. 23, 2002, pp. 606-608.

[14] D. Pogany , S. Bychikhin, J. Kuzmik , V. Dubec , N. Jensen , M. Denison, G. Groos, M. Stecher and E. Gornik, "Investigation of thermal distribution during destructive pulses in ESD protection devices using a single-shot, nanosecond resolution, two-dimensional interferometric method", In *IEDM'2002 Techn. Digest*, pp. 345-348.

[15] C. Fürböck, K. Esmark, M. Litzenberger, D. Pogany, G. Groos, R. Zelsacher, M. Stecher, and E. Gornik, "Thermal and free carrier concentration mapping during ESD event in smart power ESD protection devices using an improved laser interferometric technique", *Microel. Reliab*., vol. 40, 2000, pp. 1365-1370.

[16] D. Pogany, S. Bychikhin, C. Fürböck, M. Litzenberger, E. Gornik, G. Groos, K. Esmark, M. Stecher, "Quantitative internal thermal energy mapping of semiconductor devices under short current stress using backside laser interferometry", *IEEE Trans. Electron Devices*, vol. 49, 2002, pp. 2070-2079.

[17] K. Esmark, C. Fürböck, H. Gossner, G. Groos, M. Litzenberger, D. Pogany, R. Zelsacher, M. Stecher, and E. Gornik, "Simulation and experimental study of temperature distribution during ESD stress in smart-power technology ESD protection devices", In *Proc. IRPS'2000*, pp. 304-309.

[18] S. Bychikhin, M. Litzenberger, P. Kamvar, C. Fürböck, D. Pogany, E. Gornik, G. Groos, M. Stecher, "Laser interferometric mapping of smart power ESD protection devices with different blocking capabilities", In *Proc. ESSDERC'2001*, pp. 231-234.

[19] D. Pogany, S. Bychikhin, M. Litzenberger, E. Gornik, G. Groos and M. Stecher, "Extraction of spatio-temporal distribution of power dissipation in semiconductor devices using nanosecond interferometric mapping technique", *Appl. Phys. Lett*., vol. 81, 2002, pp. 2881-2883.

[20] D. Pogany, M. Litzenberger, S. Bychikhin, E. Gornik, G. Groos, M. Stecher, "A method for extraction of power dissipating sources from interferometric thermal mapping measurements", In *Proc. ESSDERC'2002*, pp. 243-246.

[21] T. J. Maloney, and N. Khurana, "Transmission line pulsing techniques for circuit modeling of ESD phenomena", In *Proc. EOS/ESD Symp. 1985*, pp. 49-54.

[22] K. G. McKay, "Avalanche breakdown in silicon", *Phys. Rev.*, vol. 94, 1954, pp. 877-884.

[23] P. Salome, C. Leroux, D. Mariolle, D. Lafond, J. P. Chante, P. Crevel, G. Reimbold: "An attempt to explain thermally induced soft failures during low level ESD stresses: study of the differences between soft and hard NMOS failures", *Microel. Reliab*., vol. 38, 1998, pp. 1763-1772.